Letter | Editors' Suggestion

Phase-sensitive quantum spectroscopy with high-frequency resolution

Nicolas Staudenmaier,[1] Simon Schmitt,[1] Liam P. McGuinness,[1,2,*] and Fedor Jelezko[1,3]

[1]*Institute for Quantum Optics, Ulm University, D-89081 Ulm, Germany*

[2]*Laser Physics Centre, Research School of Physics, Australian National University, Acton, Australian Capital Territory 2601, Australia*

[3]*Center for Integrated Quantum Science and Technology, Ulm University, D-89081 Ulm, Germany*

(Received 14 May 2021; accepted 27 July 2021; published 30 August 2021)

Classical sensors for spectrum analysis are widely used but lack micro- or nanoscale spatial resolution. On the other hand, quantum sensors, capable of working with nanoscale precision, do not provide precise frequency resolution over a wide range of frequencies. Using a single spin in diamond, we present a measurement protocol for quantum probes which enables full signal reconstruction on a nanoscale spatial resolution up to potentially 100 GHz. We achieve 58 nT/$\sqrt{\text{Hz}}$ amplitude and 0.095 rad/$\sqrt{\text{Hz}}$ phase sensitivity and a relative frequency uncertainty of 10^{-12} for a 1.51 GHz signal within 10 s of integration. This technique opens the way to quantum spectrum analysis methods with potential applications in electron spin detection and nanocircuitry in quantum technologies.

DOI: 10.1103/PhysRevA.104.L020602

Spectrum analysis, whereby phase, amplitude, or frequency information is extracted from periodic signals, is a widespread tool underpinning applications ranging from imaging and microscopy [1], chemical identification [2–4], development of time and frequency standards [5], quantum state tomography [6], radar detection [7], and medical diagnosis [8,9]. As a physical measurement is required to provide information to spectral estimation algorithms, their ultimate accuracy is governed by physical laws with limits given by quantum mechanics. Detectors made up of individual atoms thereby allow information encoded in such spectra to be obtained at the limits of sensitivity, resolution, and noninvasiveness.

Here, we construct a protocol which allows a single quantum coherent spin to form a heterodyne detector (quantum analog of the classical heterodyne detector) for near-resonant fields. We extend techniques recently developed to improve the spectral resolution at low frequencies <100 MHz based on dynamical decoupling [10–12], to high frequencies in the microwave regime where existing methods for microwave detection are limited in terms of spatial or spectral resolution [13–15]. We use single spins associated with nitrogen-vacancy (NV) centers in diamond to perform spectroscopy of magnetic fields oscillating at gigahertz frequencies, close to the spin resonance frequency. At the nanoscale, single NV centers have allowed for nuclear magnetic resonance and electron paramagnetic resonance spectroscopy of single molecules and nuclei to be performed [16–18]. Importantly, by recording the frequency of the magnetic field, structural and spatial information of the sample can be obtained [2,3,17,18]. Applications of the presented technique could be for the detection of single electron spins [16,19], spin waves of magnons [20], characterization of miniaturized electric circuits for communication and quantum technologies [21], and (Doppler) radar detection [22].

While the analogy to classical heterodyne detection is not perfect, the protocol preserves many of the same hallmarks, namely, (1) down-conversion of high-frequency signals to a bandwidth within the readout bandwidth, (2) simultaneous recording of phase, amplitude, and frequency information, allowing for complete signal reconstruction, and (3) frequency resolution limited by the stability of an external clock, which is detector independent. We demonstrate each of these characteristics by constructing an atomic heterodyne detector from a single quantum coherent spin.

The idea is to tailor the sensor-signal interaction in such a way that the result of each measurement depends on the phase of the signal. This is done by introducing a local oscillator which can be used to obtain a beat note with the signal. We refer to the technique as high-frequency Qdyne (where Qdyne stands for quantum heterodyne) due to the analogy to classical heterodyne detection but with a quantum sensor [10]. Note that this technique is different from recent methods requiring dynamical decoupling as here no qubit control is performed during the sensing duration [10,11,23,24]. Methods for low-frequency detection rely on dynamical decoupling methods where the sensor accumulates a phase that is transferred into different populations. In our approach instead the signal directly drives the sensor transition. Hence, there is no need to employ dynamical decoupling. Analogs to another technique [23,25] can be drawn, although here we use a distinct protocol which is immediately applicable of sensing of continuous fields. In the present Letter we focus on the phase-resolving capabilities and characterize the protocol's performance for spectrum analysis.

High-frequency Qdyne technique. The magnetic field of a near-resonant signal is described with a time-varying function of $B(t) = B_0 \cos(2\pi \nu_{\text{sig}} t + \phi_0)$ with an unknown

*liam.mcguinness@anu.edu.au

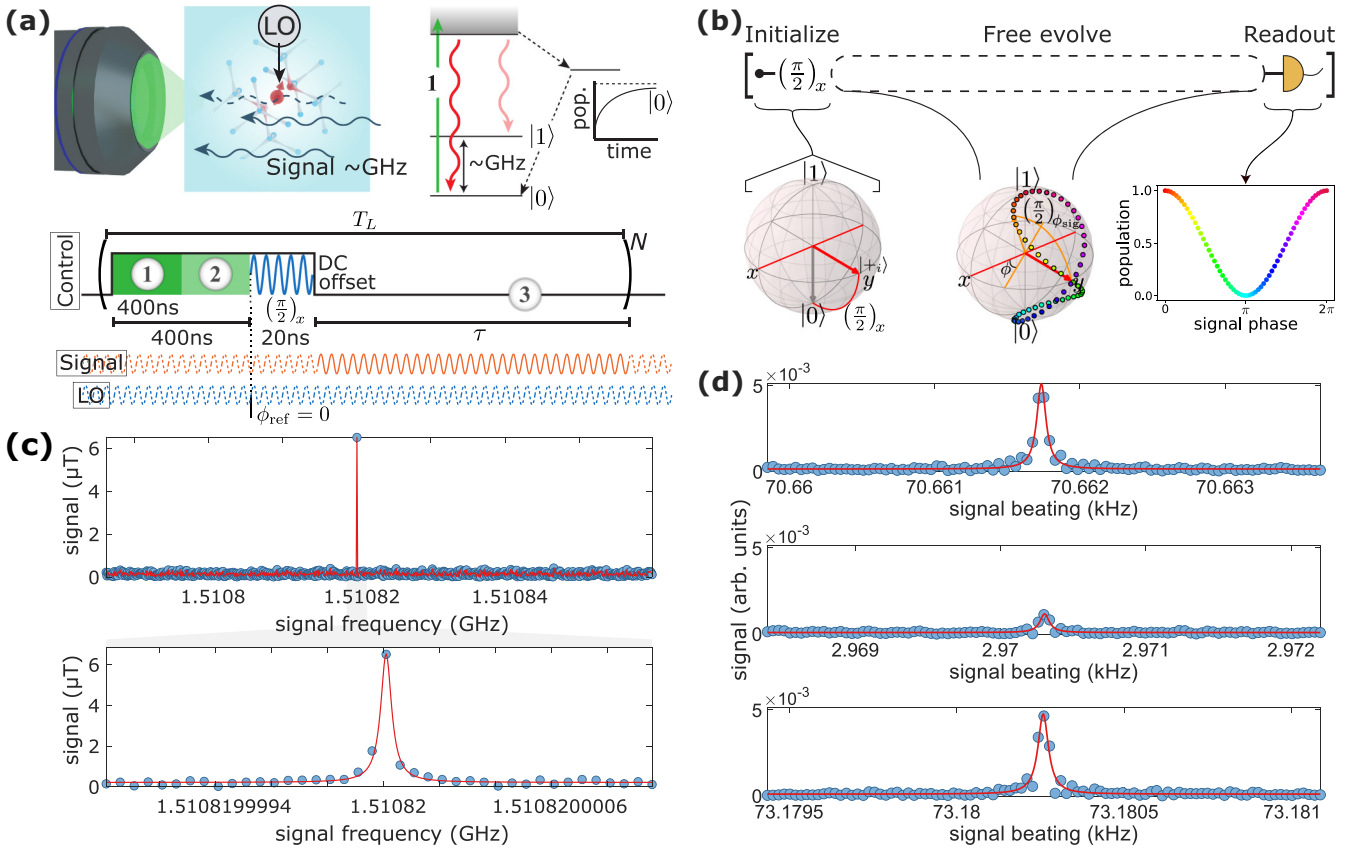

FIG. 1. Nanoscale high-frequency sensing. (a) Confocal setting for sensing with a single NV center in diamond. The right panel shows its level structure and the lower panel the pulse sequence for high-frequency Qdyne. (1) The NV center is excited with a green laser and the fluorescence is collected. (2) Population decay via a metastable state initializes the NV center in $|0\rangle$. (3) A DC shift can be applied to drive the sensor out of resonance with respect to the signal. The offset is turned off for a time τ to allow interaction with the sensor. The single sequence length of duration T_L is repeated many times. (b) Working principle of the high-frequency Qdyne method. After preparation of $|+_i\rangle$ with a $\pi/2$ pulse around the x axis the final state after signal interaction depends on the signal phase ϕ. A signal interaction resulting in a $\pi/2$ rotation is shown. The states are shown on the Bloch sphere in the rotating frame of the local oscillator. (c) Measurement of a 1.510 82 GHz signal. In a sampling time of 10 s, 3×10^6 samples are taken that correspond to 1.5×10^6 frequency channels in the FFT (only every 2000th point is shown). Lower plot: Zoom around the peak. (d) Measurement with a signal being applied only during the sensing period (top) and having a continuous signal without (center) and with a DC shift (bottom). The x axis is the absolute value $\delta = |\delta_0|$ of the beat note of Eq. (5).

amplitude B_0, phase ϕ_0, and frequency $\nu_{\rm sig}$. In the rotating frame the interaction Hamiltonian with a two-level system is written as

$$H = \frac{\hbar\Delta}{2}\sigma_z + \frac{\hbar\Omega_{\rm sig}}{2}\sigma_{\phi_0}, \tag{1}$$

where $\sigma_{\phi_0} = \cos\phi_0\,\sigma_x + \sin\phi_0\,\sigma_y$, the Pauli matrices σ_i, the driving amplitude $\Omega_{\rm sig} = \sqrt{\Delta^2 + \Omega_0^2}$ with detuning $\Delta = 2\pi(\nu_{\rm sig} - \nu_{\rm sens})$, the frequency difference between the signal and the sensor's resonance $\nu_{\rm sens}$, and $\Omega_0 = \gamma_{\rm sens}B_0$ (gyromagnetic ratio $\gamma_{\rm sens}$ of the sensor).

To sense this signal we use a single nitrogen-vacancy (NV) center in diamond. Its spin ground state can be effectively described as a two-level system with states $|0\rangle$ and $|1\rangle$. Readout is done optically with a green laser and collecting the spin-dependent fluorescence [see Fig. 1(a)]. After initialization in $|0\rangle$, the NV center is prepared in the superposition state $|+_i\rangle = \frac{1}{\sqrt{2}}(|0\rangle + i|1\rangle)$ by a $\pi/2$ pulse around the x axis by a reference pulse with a known phase. This state then evolves under the action of the near-resonant signal field for some time τ. The protocol is constructed such that the reference pulse always has the phase $\phi_{\rm ref} = 0$ and for every subsequent repetition the same state $|+_i\rangle$ is prepared. We note that this is not a stringent requirement for the protocol, since it can also be achieved with a signal generator where $\phi_{\rm ref}$ changes according to the control frequency, but as presented here it is mathematically streamlined, and experimentally achievable using an arbitrary waveform generator.

In the following, if not otherwise stated, we toggle the signal on during the τ interval, and off for the remaining time (as performed in Ref. [23]) with a switch. However, for many spectroscopy applications one may not have control over the signal. To circumvent signal deterioration for continuous fields (especially for strong signals) one can apply a DC magnetic field that shifts the sensor transition out of resonance during state preparation and readout.

Assuming the signal interaction only occurs during τ, the population in $|1\rangle$ of the final state is calculated to be

$$|c_1|^2 = \frac{1}{2}\left[1 - \frac{\Delta\Omega_0}{\Omega_{\rm sig}^2}[1-\cos(\Omega_{\rm sig}\tau)]\sin(\phi) + \frac{\Omega_0}{\Omega_{\rm sig}}\sin(\Omega_{\rm sig}\tau)\cos(\phi)\right], \quad (2)$$

where $\phi = \phi(t) = 2\pi\nu_{\rm sig}t + \phi_0$ is an instantaneous phase of the signal at some time t. For the calculation of this result, see the Supplemental Material (SM) [26]. Assuming small detuning, $\Delta \ll \Omega_0$, Eq. (2) is approximated as

$$|c_1|^2 \approx \tfrac{1}{2}[1+\sin(\Omega_0\tau)\cos(\phi)]. \quad (3)$$

Experimentally, the spin population is sampled at fixed time intervals T_L such that the signal phase ϕ changes by a constant increment and each outcome is stored individually. It is this synchronization of single measurements at a rate of $1/T_L$, in addition to the $\phi_{\rm ref}$, that defines the local oscillator (LO) frequency:

$$\nu_{\rm LO} = \frac{\text{round}(\nu_{\rm sens}T_L)}{T_L} = \frac{N_{\rm LO}}{T_L}. \quad (4)$$

$N_{\rm LO} = \text{round}(\nu_{\rm sens}T_L)$ is the rounded integer number of periods of the sensor resonance frequency $\nu_{\rm sens}$ within T_L and the number that defines the closest local oscillator frequency to a signal frequency that is within the linewidth of the sensor. A detailed discussion of the local oscillator can be found in the SM [26]. We emphasize that the local oscillator could also be defined by a control field that is used to manipulate the NV center at resonance with a continuously updating phase [23,25], but then a reference phase $\phi_{\rm ref} \neq 0$ has to be considered for each measurement.

Sampling at times $T_n = nT_L$, the populations $|c_{1,n}|^2$ are calculated from Eq. (2) [or (3)] with phases $\phi_n = \phi_0 + 2\pi\, T_n\delta_0$ where the phase increment is determined by the beating of the signal against the local oscillator,

$$\delta_0 = \nu_{\rm sig} - \nu_{\rm LO}. \quad (5)$$

As a result, the outcome probability of each measurement oscillates with frequency δ_0.

To show the working principle, a diamond sample fabricated into a solid immersion lens that is overgrown with a 100-nm-thick layer of isotopically purified ^{12}C is used. The high purity allows the NV center to reach dephasing times up to 50 μs. An external magnetic field is aligned along the NV axis to about 50 mT. The sample is mounted in a confocal microscope setup that is controlled via the software suite QUDI [27]. In Fig. 1(c), a 1.51 GHz signal (approximately NV resonance frequency) is measured and a fast Fourier transform (FFT) resolves the oscillation in the sampled data. After preparing $|+_i\rangle$ the signal of 6.5 μT amplitude interacts with the NV center for 1404 ns and in an integration time of 10 s, 3×10^6 samples are obtained. From the local oscillator the frequency channels of the FFT can be assigned to the scanned spectrum.

In Fig. 1(d), we compare the measured spectrum when the signal is toggled on and off, as opposed to applied continuously. In the upper panel, the signal is only on during τ, and in the middle panel, the signal remains on continuously. In the lower panel, the signal is applied continuously, but the NV center is shifted out of resonance by application of a DC shift which is only turned off during τ. The DC shift is created by applying a constant current to the NV center control stripline which causes a magnetic field of 1 G at the NV center and shifts the resonance frequency by 3 MHz. As the control $\pi/2$ pulse is much stronger than the sensing field, only the signal is brought out of resonance by the DC shift. We find that a continuously applied signal but with DC control gives comparable results to one toggled on/off, while it significantly reduces the measurement signal without DC control.

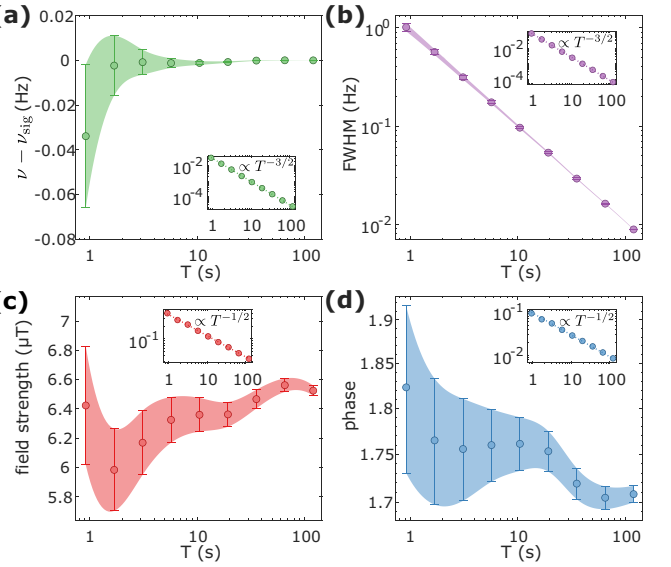

FIG. 2. Full signal reconstruction. (a), (c), (d) Signal frequency, strength, and phase estimation. Measuring all three parameters allows full reconstruction of the signal. In (a) the difference between the estimated frequency ν and the signal frequency $\nu_{\rm sig}$ is displayed. (b) Linewidth (full width at half maximum) $\Delta\nu = 1/T$. The insets show the uncertainty of the respective estimation (error bars) as the 95% confidence intervals of the fit parameters. (a), (b) scale with $T^{-3/2}$ and (c), (d) with $T^{-1/2}$.

Signal reconstruction. Analysis of the discrete Fourier transform, just as in classical heterodyne detection, allows for full signal reconstruction. In Fig. 2, an estimation of the signal parameters after different integration times is shown for the same signal as shown in Fig. 1(c). Frequency and amplitude [Figs. 2(a) and 2(c)] are estimated with a Lorentzian fit on the peak in the FFT. The uncertainty is obtained from the 95% confidence interval of the fit. Importantly, frequency uncertainty scales as $T^{-3/2}$ as a product of reduced noise ($T^{-1/2}$) and reduced linewidth ($1/T$) as a function of total measurement time T. A precision <1 mHz is achieved after 10 s integration time, resulting in a relative frequency uncertainty $\frac{\delta\nu}{\nu} < 10^{-12}$. Ultimately, the resolution and uncertainty are limited by the stability of the clock which times the arbitrary waveform generator, i.e., the local oscillator defined via the sequence length produced by the arbitrary waveform generator. As the timing is given to an accuracy 10^{-7} the estimated signal frequency may be systematically shifted from the actual frequency. As a result, the analysis only includes statistical errors and not systematic ones.

For phase estimation due to the finite resolution in the FFT spectrum, the signal phase is estimated from the phases at the two frequency channels next to the estimated peak (obtained from the argument of the complex-valued FFT). Then, with linear interpolation the phase of the beat note is obtained, from which the initial signal phase ϕ_0 can be recovered because the local oscillator's reference is $\phi_{\text{ref}} = 0$. Note that for a detuned signal the estimated phase can be different from the signal phase ϕ_0. From Eq. (2) one can see that the beat note is the sum of a sine and cosine. The resulting oscillation has the same frequency but not necessarily the same phase ϕ. In our measurements the signal detuning Δ is small and this effect can be neglected [see Eq. (3)]. In the SM [26] a detailed analysis of this phase shift is included.

Attention has to be given to the sign of δ_0 in Eq. (5). If $\delta_0 < 0$, a negative frequency is sampled. Thus, the signal phase is the negative of the estimated one from the FFT. Furthermore, frequency estimation might not be unique because it does not distinguish between negative and positive frequency. The observed signal has the frequency $\delta = |\delta_0| = |\nu_{\text{sig}} - \nu_{\text{LO}}|$. This ambiguity can be resolved with a second measurement as outlined in the SM [26].

Spectrum analysis benchmarks. The measurement technique allows for spectrum analysis on the nanoscale as it employs an atomic-sized sensor that can be used to estimate signals within a wide frequency range. To understand the capabilities that arise with the technique we investigate some benchmarks of this protocol.

Standard quantum sensing protocols usually rely on the pointwise accumulation of spectral information [28]. In contrast, this technique makes intrinsic use of the FFT mode with a sample rate $1/T_L$. In this way, information over many frequency channels is sampled over the measurement time. This allows the sensitivity to be increased by minimizing dead time. In Fig. 3(a) the noise floor in the FFT spectrum of a measurement with 223 nT signal strength is shown from which a sensitivity of 58 nT/$\sqrt{\text{Hz}}$ is obtained (noise floor at $T = 1$ s). From the data of Fig. 2 we calculate a sensitivity of 0.095 rad/$\sqrt{\text{Hz}}$ for phase and 0.03 Hz/Hz$^{3/2}$ for frequency estimation. We want to emphasize that no dynamical decoupling is incorporated here. High-frequency pulsed [29] or continuous decoupling [30] offer the potential to further increase the amplitude sensitivity to 4 nT/$\sqrt{\text{Hz}}$ [31].

We further investigate the spectral and dynamic range and bandwidth of the technique. The operating range can be extended from megahertz (or even less) to high frequency (>GHz) by tuning the resonance of the sensor. For the NV center a range from 1 to 5 GHz can be covered with static magnetic fields up to 70 mT and 100 GHz are reached with a 3.5 T field [32,33]. The upper limit to the operating range is set by technical challenges that are involved for generating stable high magnetic fields and handling high-frequency microwaves, the lower limit is set simply by the integration time $1/T$.

The dynamic range is set by the sensor properties and integration time. An upper limit can be clearly defined because each interaction with a signal which results in a rotation of more than $\pi/2$ of the sensor state cannot be distinguished from a rotation less than $\pi/2$. For that reason we set the upper

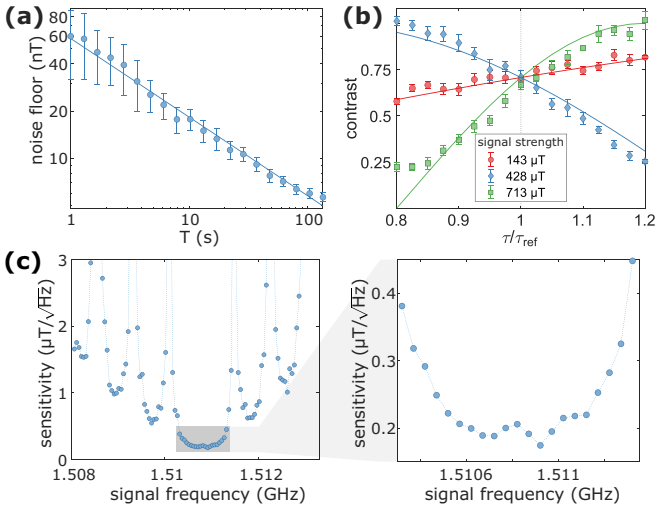

FIG. 3. (a) Noise floor in dependence on integration time. Amplitude sensitivity of the measurement is obtained from a fit of slope $T^{-1/2}$ that gives a 58 nT noise floor at $T = 1$ s. (b) Example of signal strength ambiguities for an interaction length $\tau_{\text{ref}} = 31.3$ ns. These ambiguities are lifted when the interaction time is changed. (c) Sensitivity in dependence on the signal frequency. Signals of strength 6.5 μT with varying frequency are detected. All other measurement parameters are kept constant.

end of the dynamic range to the signal strength at which a $\pi/2$ rotation of the sensor within $\tau = T_2^*/2$ (the sensing time for which best sensitivity is obtained [28]) is performed, $B_{\text{max}} = \frac{\pi}{\gamma_{\text{NV}} T_2^*}$. With $\gamma_{\text{NV}} = 2\pi \times 28.03$ MHz/mT and $T_2^* = 50$ μs we have $B_{\text{max}} = 0.36$ μT. However, one always has the freedom to increase the dynamic range by setting $\tau < T_2^*/2$ at the expense of a reduced sensitivity as is done in the measurement of Fig. 1(c). By using multiple measurements with different τ it is also possible to increase the dynamic range because ambiguities for a rotation larger and smaller than $\pi/2$ get resolved, and with a lower trade-off in reduced sensitivity. This is measured for three different signal strengths in Fig. 3(b) that result in the same measurement signal for an interaction time of $\tau_{\text{ref}} = 31.3$ ns. The lower end of the dynamic range is simply given by the sensitivity, since this is the minimum field strength that can be identified. The full dynamic range for a single measurement is now 58 nT$\times\sqrt{T/1\text{ s}}$ (total integration time T) to 360 nT for $\tau = T_2^*/2 = 25$ μs.

The bandwidth is naturally given by the linewidth of the sensor's transition and is limited by the dephasing time $\Delta\nu_b = 1/T_2^*$. However, the bandwidth might be reduced if temporal overheads are involved for preparation or readout of the sensor. In these cases a unique assignment of the frequency within the sensor's linewidth might not be possible, due to undersampling. If the sequence length exceeds the dephasing time, $T_L = \tau + t_{\text{overhead}} > T_2^*$, the sampling rate limits the effective bandwidth $\Delta\nu_b = 1/T_L$. Note that we distinguish between positive and negative δ_0 and that the sampling theorem $\delta_{\text{max}} = \delta_{0,\text{max}} = -\delta_{0,\text{min}} = 1/2T_L$ is always satisfied. Furthermore, for a very weak signal, the condition $\Omega_0 > \Delta$ may not be satisfied, although the signal frequency lies within the detector bandwidth. Thus the signal strength can also define the bandwidth as $\Omega_0/2\pi$.

In Fig. 3(c) the sensitivity is measured in dependence of the signal frequency while all other measurement parameters are kept constant. The protocol is susceptible also to frequencies outside of the sensor linewidth but with a reduced sensitivity. In the SM [26] we present a method to overcome potential ambiguities.

In comparison to classical spectrum analyzers this quantum analog yields some specific peculiarities. While classical devices can have better sensitivity they are much larger in size and operate far from nanoscale spatial resolution. As an atomic-sized defect in the diamond lattice, the NV centers (or other appropriate quantum sensors) are able to measure small signals on the nanoscale with nanometer spatial resolution. In order to be sensitive to a certain frequency bandwidth, an external magnetic field has to be adjusted correctly. Classical frequency-swept analyzers can cover a large bandwidth by applying band-limited electrical filters. The drawback in this case is that the analyzer may require a long time to record the spectrum step by step. FFT mode analyzers on the other side yield a bandwidth that is given by the sampling rate. Our quantum spectrum analyzer also operates in FFT mode and the bandwidth is given by either the sensor linewidth or the sampling rate. Applying this Qdyne technique to the work of Chipaux *et al.* [13] where a magnetic field gradient is used with an NV center ensemble, a wide frequency range can be covered with the drawback of reducing nanoscale to microscale resolution.

Discussion. We have presented a powerful measurement technique that extends high-frequency resolution quantum sensing to high-frequency oscillating fields. In analogy to classical heterodyne detection, full signal reconstruction is possible as frequency, amplitude, and phase information is provided. We obtain a phase sensitivity of $0.095\ \mathrm{rad}/\sqrt{\mathrm{Hz}}$. Detailed analyses of the spectral and dynamic range show possibilities and limitations of spectrum analyses for different signals and can be adapted to various probes used as quantum sensors. The detection of highly coherent signals will benefit from the technique especially in settings on the nanoscale such as miniaturized integrated circuits for communication or quantum technologies. Velocimetry in Doppler radar detection for velocities down to a few $\mu\mathrm{m/s}$ [34] in nano- to microscale settings will be possible owing to the high spectral resolution and phase sensitivity. Methods to increase the spectral and dynamic range are presented that allow one to overcome some of their limitations with the help of a second measurement. Employing NV center ensembles with a high magnetic field gradient could be used to considerably increase the bandwidth of the method.

Acknowledgments. We acknowledge fruitful discussions with Genko T. Genov. This work is supported by the Australian Research Council, Future Fellowship (FT180100100) (L.P.M.), the Bosch Forschungsstiftung (N.S. and F.J.), the European Research Council via Synergy Grant HyperQ, the German Research Foundation (excellence cluster POLIS and CRC1279), the German Federal Ministry of Education and Research, and the European Commission via ASTERIQS (F.J.).

[1] E. Betzig and J. K. Trautman, Near-field optics: microscopy, spectroscopy, and surface modification beyond the diffraction limit, Science **257**, 189 (1992).

[2] W. P. Aue, E. Bartholdi, and R. R. Ernst, Two-dimensional spectroscopy. Application to nuclear magnetic resonance, J. Chem. Phys. **64**, 2229 (1976).

[3] K. Wüthrich, The way to NMR structures of proteins, Nat. Struct. Biol. **8**, 923 (2001).

[4] H. W. Spiess, NMR spectroscopy: Pushing the limits of sensitivity, Angew. Chem. Int. Ed. **47**, 639 (2008).

[5] S. A. Diddams, J. C. Bergquist, S. R. Jefferts, and C. W. Oates, Standards of time and frequency at the outset of the 21st century, Science **306**, 1318 (2004).

[6] S. Lloyd, M. Mohseni, and P. Rebentrost, Quantum principal component analysis, Nat. Phys. **10**, 631 (2014).

[7] T. M. Turpin, Spectrum analysis using optical processing, Proc. IEEE **69**, 79 (1981).

[8] P. C. Lauterbur, Image formation by induced local interactions: Examples employing nuclear magnetic resonance, Nature (London) **242**, 190 (1973).

[9] R. Bowtell, Medical imaging – a colourful future for MRI, Nature (London) **453**, 993 (2008).

[10] S. Schmitt, T. Gefen, F. M. Stürner, T. Unden, G. Wolff, C. Müller, J. Scheuer, B. Naydenov, M. Markham, S. Pezzagna, J. Meijer, I. Schwarz, M. Plenio, A. Retzker, L. P. McGuinness, and F. Jelezko, Submillihertz magnetic spectroscopy performed with a nanoscale quantum sensor, Science **356**, 832 (2017).

[11] J. M. Boss, K. S. Cujia, J. Zopes, and C. L. Degen, Quantum sensing with arbitrary frequency resolution, Science **356**, 837 (2017).

[12] D. R. Glenn, D. B. Bucher, J. Lee, M. D. Lukin, H. Park, and R. L. Walsworth, High-resolution magnetic resonance spectroscopy using a solid-state spin sensor, Nature (London) **555**, 351 (2018).

[13] M. Chipaux, L. Toraille, C. Larat, L. Morvan, S. Pezzagna, J. Meijer, and T. Debuisschert, Wide bandwidth instantaneous radio frequency spectrum analyzer based on nitrogen vacancy centers in diamond, Appl. Phys. Lett. **107**, 233502 (2015).

[14] A. Horsley and P. Treutlein, Frequency-tunable microwave field detection in an atomic vapor cell, Appl. Phys. Lett. **108**, 211102 (2016).

[15] A. Horsley, P. Appel, J. Wolters, J. Achard, A. Tallaire, P. Maletinsky, and P. Treutlein, Microwave Device Characterization Using a Widefield Diamond Microscope, Phys. Rev. Applied **10**, 044039 (2018).

[16] M. S. Grinolds, S. Hong, P. Maletinsky, L. Luan, M. D. Lukin, R. L. Walsworth, and A. Yacoby, Nanoscale magnetic imaging of a single electron spin under ambient conditions, Nat. Phys. **9**, 215 (2013).

[17] H. J. Mamin, M. Kim, M. H. Sherwood, C. T. Rettner, K. Ohno, D. D. Awschalom, and D. Rugar, Nanoscale nuclear magnetic resonance with a nitrogen-vacancy spin sensor, Science **339**, 557 (2013).

[18] T. Staudacher, F. Shi, S. Pezzagna, J. Meijer, J. Du, C. A. Meriles, F. Reinhard, and J. Wrachtrup, Nuclear magnetic

resonance spectroscopy on a (5-nanometer)^3 sample volume, Science **339**, 561 (2013).

[19] L. T. Hall, P. Kehayias, D. A. Simpson, A. Jarmola, A. Stacey, D. Budker, and L. C. L. Hollenberg, Detection of nanoscale electron spin resonance spectra demonstrated using nitrogen-vacancy centre probes in diamond, Nat. Commun. **7**, 10211 (2016).

[20] A. Finco, A. Haykal, R. Tanos, F. Fabre, S. Chouaieb, W. Akhtar, I. Robert-Philip, W. Legrand, F. Ajejas, K. Bouzehouane, N. Reyren, T. Devolder, J.-P. Adam, J.-V. Kim, V. Cros, and V. Jacques, Imaging non-collinear antiferromagnetic textures via single spin relaxometry, Nat. Commun. **12**, 767 (2021).

[21] J. C. Bardin, D. H. Slichter, and D. J. Reilly, Microwaves in quantum computing, IEEE J. Microw. **1**, 403 (2021).

[22] C. Alabaster, *Pulse Doppler Radar: Principles, Technology, Applications* (SciTech Publishing, Edison, NJ, 2012).

[23] J. Meinel, V. Vorobyov, B. Yavkin, D. Dasari, H. Sumiya, S. Onoda, J. Isoya, and J. Wrachtrup, Heterodyne sensing of microwaves with a quantum sensor, Nat. Commun. **12**, 2737 (2021).

[24] S. Pang and A. N. Jordan, Optimal adaptive control for quantum metrology with time-dependent Hamiltonians, Nat. Commun. **8**, 14695 (2017).

[25] Y. Chu, P. Yang, M. Gong, M. Yu, B. Yu, M. B. Plenio, A. Retzker, and J. Cai, Precise Spectroscopy of High-Frequency Oscillating Fields with a Single-Qubit Sensor, Phys. Rev. Applied **15**, 014031 (2021).

[26] See Supplemental Material at http://link.aps.org/supplemental/10.1103/PhysRevA.104.L020602 for details to the experimental setup and extended analysis and discussion of the measurement protocol.

[27] J. M. Binder, A. Stark, N. Tomek, J. Scheuer, F. Frank, K. D. Jahnke, C. Müller, S. Schmitt, M. H. Metsch, T. Unden, T. Gehring, A. Huck, U. L. Andersen, L. J. Rogers, and F. Jelezko, Qudi: A modular python suite for experiment control and data processing, SoftwareX **6**, 85 (2017).

[28] C. L. Degen, F. Reinhard, and P. Cappellaro, Quantum sensing, Rev. Mod. Phys. **89**, 035002 (2017).

[29] T. Joas, A. M. Waeber, G. Braunbeck, and F. Reinhard, Quantum sensing of weak radio-frequency signals by pulsed Mollow absorption spectroscopy, Nat. Commun. **8**, 964 (2017).

[30] A. Stark, N. Aharon, T. Unden, D. Louzon, A. Huck, A. Retzker, U. L. Andersen, and F. Jelezko, Narrow-bandwidth sensing of high-frequency fields with continuous dynamical decoupling, Nat. Commun. **8**, 1105 (2017).

[31] G. Balasubramanian, P. Neumann, D. Twitchen, M. Markham, R. Kolesov, N. Mizuochi, J. Isoya, J. Achard, J. Beck, J. Tissler, V. Jacques, P. R. Hemmer, F. Jelezko, and J. Wrachtrup, Ultralong spin coherence time in isotopically engineered diamond, Nat. Mater. **8**, 383 (2009).

[32] V. Stepanov, F. H. Cho, C. Abeywardana, and S. Takahashi, High-frequency and high-field optically detected magnetic resonance of nitrogen-vacancy centers in diamond, Appl. Phys. Lett. **106**, 063111 (2015).

[33] N. Aslam, M. Pfender, R. Stöhr, P. Neumann, M. Scheffler, H. Sumiya, H. Abe, S. Onoda, T. Ohshima, J. Isoya, and J. Wrachtrup, Single spin optically detected magnetic resonance with 60–90 GHz (E-band) microwave resonators, Rev. Sci. Instrum. **86**, 064704 (2015).

[34] M. Jing, Y. Hu, J. Ma, H. Zhang, L. Zhang, L. Xiao, and S. Jia, Atomic superheterodyne receiver based on microwave-dressed Rydberg spectroscopy, Nat. Phys. **16**, 911 (2020).